

## Dissipative solitons and antisolitons

A. Ankiewicz<sup>a</sup>, N. Devine<sup>a</sup>, N. Akhmediev<sup>a</sup>, J.M. Soto-Crespo<sup>b,\*</sup>

<sup>a</sup> Optical Sciences Group, Research School of Physical Sciences and Engineering, The Australian National University, Canberra ACT 0200, Australia

<sup>b</sup> Instituto de Óptica, C.S.I.C., Serrano 121, 28006 Madrid, Spain

Received 29 May 2007; accepted 2 June 2007

Available online 6 June 2007

Communicated by V.M. Agranovich

### Abstract

Using the method of moments for dissipative optical solitons, we show that there are two disjoint sets of fixed points. These correspond to stationary solitons of the complex cubic–quintic Ginzburg–Landau equation with concave and convex phase profiles respectively. Numerical simulations confirm the predictions of the method of moments for the existence of two types of solutions which we call solitons and antisolitons. Their characteristics are distinctly different.

© 2007 Elsevier B.V. All rights reserved.

PACS: 42.65.-k; 47.20.Ky; 47.25.Qv

The complex Ginzburg–Landau equation (CGLE) describes a variety of phenomena in physics, chemistry and biology. The diversity of systems to which this equation can be applied is so large that this sphere of knowledge has been called “The world of the Ginzburg–Landau equation” [1]. The huge number of assorted solutions to this equation [1–4] is just the other side of this world. In nonlinear dynamical systems, a variation of the parameters of the system changes the types of solutions via bifurcations. As there are at least five parameters in the CGL equation, the number of solutions and bifurcations can really be enormous. The extent of the solutions is remarkably large, even if we restrict ourselves to self-localized solutions of the CGLE, which belong to the class of “dissipative solitons” [5].

In this work, once again, we confirm that our knowledge of dissipative solitons of the CGLE is far from being complete, even in the case of one-dimensional solitons. We consider here the simplest case of stationary 1-D solitons where each has a plain bell-shaped profile with a single maximum. For this simple case, we expect to have the property of soliton continuity, i.e. two stationary bell-shaped solitons that belong to two different points in the parameter space would be continuously

transformed into each other when changing the parameters of the system. However, it turns out that this is not the case! There are two distinctively different areas where two different types of dissipative solitons exist. There is no way of continuously transforming a soliton from one region into a soliton of the other region.

The lack of general analytical solutions for the complex cubic–quintic CGLE leads us to the necessity of using simple approaches to explore the existence of certain class of solutions. One of the low-dimensional approximations that can be used for finding CGLE solitons is the method of moments, combined with the use of simple trial functions. For plain bell-shaped solitons, the use of a trial function with only three parameters has proved to be a reasonably good approximation and it has been justified in this particular case with the finding of two separate branches of solitons. We confirm the existence of these two branches using direct numerical simulations of the CGLE.

Our studies are based on an extended complex Ginzburg–Landau equation, that includes cubic and quintic nonlinear terms. This normalized propagation equation reads [6]:

$$i\psi_z + \frac{D}{2}\psi_{tt} + |\psi|^2\psi = i\delta\psi + i\epsilon|\psi|^2\psi + i\beta\psi_{tt} + i\mu|\psi|^4\psi - \nu|\psi|^4\psi, \quad (1)$$

\* Corresponding author.

E-mail address: [iodsc09@io.cfmac.csic.es](mailto:iodsc09@io.cfmac.csic.es) (J.M. Soto-Crespo).

where  $\psi(z, t)$  is the normalized envelope of the field,  $z$  and  $t$  are the propagation and temporal variables, respectively,  $D = 1$  is the dispersion coefficient,  $\nu$  is the coefficient of the quintic nonlinearity,  $\delta$  represents linear losses,  $\epsilon$  is the nonlinear gain coefficient,  $\beta$  stands for spectral filtering or gain dispersion, and  $\mu$  characterizes the saturation of the nonlinear gain.

The method of moments [7,8] consists in the reduction of the complete evolution problem with an infinite number degrees of freedom, to the evolution of a finite set of pulse characteristics. The problem of solving a partial differential equation is then reduced to solving a small set of ordinary differential equations. For a localized solution with a single maximum, the main pulse characteristics are the peak amplitude, the pulse width, the position of its center-of-mass and some phase chirp parameters. For an arbitrary localized field, we can introduce two integrals, namely the energy  $Q$  and momentum  $P$

$$Q = \int_{-\infty}^{\infty} |\psi|^2 dt, \quad P = \frac{1}{2} \int_{-\infty}^{\infty} (\psi \psi_t^* - \psi^* \psi_t) dt, \quad (2)$$

and higher-order generalized moments [7]:

$$I_1 = \int_{-\infty}^{\infty} t |\psi|^2 dt, \quad I_2 = \int_{-\infty}^{\infty} (t - t_0)^2 |\psi|^2 dt, \\ I_3 = \int_{-\infty}^{\infty} (t - t_0) (\psi^* \psi_t - \psi \psi_t^*) dt, \quad (3)$$

where  $t_0(z) = I_1/Q$ . The number of higher-order generalized momenta is infinite. To reduce the complexity of the model, we can restrict ourselves to deal with a finite number of them. Using the original equation (1), we can derive the evolution equations for the generalized moments [7]:

$$\frac{dQ}{dz} = i \int_{-\infty}^{\infty} (\psi R^* - \psi^* R) dt, \\ \frac{dP}{dz} = -i \int_{-\infty}^{\infty} (\psi_t R^* + \psi_t^* R) dt, \\ \frac{dI_1}{dz} = iDP + i \int_{-\infty}^{\infty} t (\psi R^* - \psi^* R) dt, \\ \frac{dI_2}{dz} = -iDI_3 + i \int_{-\infty}^{\infty} (t - t_0)^2 (\psi R^* - \psi^* R) dt, \\ \frac{dI_3}{dz} = 2P \frac{dt_0}{dz} + i \int_{-\infty}^{\infty} (2D|\psi|^2 - \gamma|\psi|^4) dt \\ + 2i \int_{-\infty}^{\infty} (t - t_0) (\psi_t R^* + \psi_t^* R) dt \\ + i \int_{-\infty}^{\infty} (\psi R^* + \psi^* R) dt, \quad (4)$$

where  $R[\psi] = i\delta\psi + i\epsilon|\psi|^2\psi + i\beta\psi_{tt} + i\mu|\psi|^4\psi - \nu|\psi|^4\psi$  is the right-hand-side part of Eq. (1). Eqs. (4) are quite general, i.e. they are valid for a large class of NLSE-type evolution equations, including Eq. (1) with arbitrary coefficients. Up to this point, the equations are exact if we use an exact solution of (1) for  $\psi$ .

In our low-dimensional approximation, we shall describe the pulse shape by using the total energy,  $Q$ , the width,  $f$ , and a chirp factor,  $c$ , while taking the central position along the  $t$  axis and soliton velocity to be zero. These 3 non-zero quantities can give a good representation of the soliton profile. More specifically, we shall use a higher-order Gaussian-type pulse, viz.

$$\psi(z, t) = a(m) \sqrt{\frac{Q(z)}{f(z)}} \\ \times \exp\left(-\frac{t^2}{f^2(z)} - \frac{t^4}{mf^4(z)} + ic(z)t^2 - i\omega z\right) \quad (5)$$

as a trial function for the method of moments. Our studies have shown that this function gives the best fit for the regions of existence of solitons. Here  $a(m)$  is a  $z$  independent constant, which is chosen in such a way that the integrated intensity, i.e. the total energy, is equal to  $Q$ . Hence

$$a(m) = \frac{\sqrt{2}e^{-m/8}}{m^{1/4}\sqrt{K_{1/4}(m/4)}},$$

where  $K$  is a modified Bessel function of 2nd kind. The constant  $m$  can be chosen arbitrarily, and we now set  $m = 1$ , so  $a(m) = 0.975445$ .

Substituting (5) into the set of Eqs. (4), we get a dynamical system for the variables  $Q$ ,  $f$  and  $c$ . Since the function (5) is symmetric in  $t$ , the integrals  $P$  and  $I_1$  are identically zero. The three other equations comprise a dynamical system of third order (see Refs. [9,10] for details):

$$Q_z = \frac{Q}{f^2} [2\delta f^2 - 3.737\beta - 1.158\beta c^2 f^4 + 1.433\epsilon f Q \\ + 1.1456\mu Q^2], \\ f_z = \frac{1}{f} [2.142\beta + 2cf^2 - 0.8738\beta c^2 f^4 - 0.2896\epsilon f Q \\ - 0.3254\mu Q^2], \\ c_z = \frac{1}{f^4} [6.453 - 2c^2 f^4 - 1.237 f Q - 1.319\nu Q^2 \\ - 19.62\beta f^2 c]. \quad (6)$$

Stationary solutions of (6) are given by the soliton parameters which are  $z$  independent, i.e.  $Q(z) = Q_0$ ,  $f(z) = f_0$  and  $c(z) = c_0$ . The latter case corresponds to a fixed point (FP) of the dynamical system (6). Fixed points of this three-variable dynamical system, together with the trial function (5), approximate the stationary solitons of the CGLE. Standard linearization techniques can be used to find the stability of these FPs. Unstable FPs usually correspond to unstable solitons. Stable FPs may correspond to stable solitons but this has to be confirmed by direct numerical simulations of the CGLE. This is

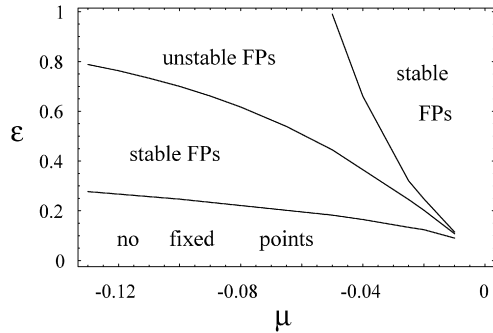


Fig. 1. Soliton bifurcation diagram on the  $\epsilon$ - $\mu$  plane. There are two regions of stable fixed points that correspond to two quite different branches of solitons. Here,  $\delta = -0.1$ ,  $\nu = -0.08$ ,  $\beta = 0.08$ .

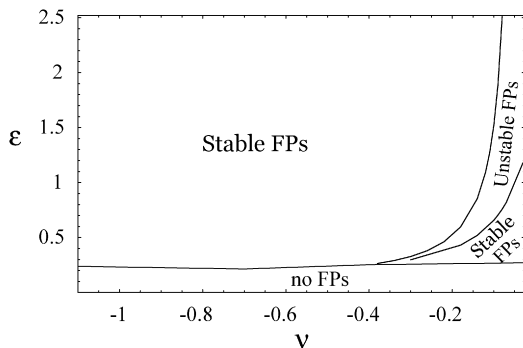


Fig. 2. Soliton bifurcation diagram on the  $\epsilon$ - $\nu$  plane. Here,  $\mu = \delta = -0.1$ ,  $\beta = 0.125$ .

related to the fact that an infinite-dimensional dynamical system has more degrees of freedom to develop a soliton instability.

Solving the dynamical system (6) for various  $\epsilon$ ,  $\mu$  and  $\nu$ , we constructed regions of stable and unstable fixed points in the space of these three parameters of the CGLE. In order to keep the presentation of the results reasonably simple, we keep  $D$ ,  $\delta$  and  $\beta$  fixed. Two plots representing the regions of stable and unstable FPs are shown in Figs. 1 and 2. Each plot is a two-dimensional slice of the six-dimensional space of the equation parameters. Each of these plots clearly shows the existence of two separate regions of stable fixed points. A point from one region cannot be transformed into a point from the other region with a continuous change of parameters. Thus, it appears that these two regions correspond to two different types of solitons of the CGLE. One of the branches has high energy,  $Q$ , while the other one has low energy. Within the low-dimensional approximation (6), these FPs are stable in both regions. However, the results for the stability of exact CGLE solitons may differ, as we explained above.

Direct simulations of the CGLE (1) confirm our predictions made using the simple model. We have numerically solved Eq. (1) using a split-step Fourier method. Thus, the second-order derivative term in  $t$  is solved in Fourier space. All other linear and nonlinear terms in the equation are solved in real space using a fourth-order Runge–Kutta method. Most of the simulations presented in the Letter were carried out using a numerical grid of 4096 points in  $t$ . We used various values of step sizes along the spatial and temporal domains to check that the

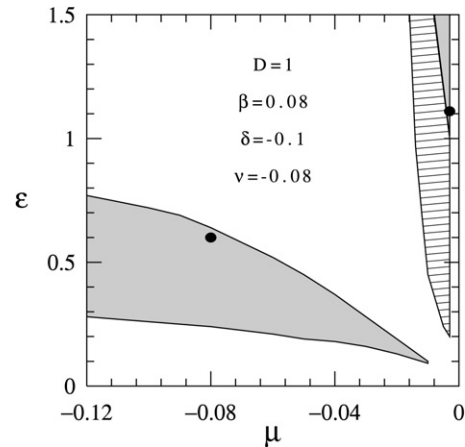


Fig. 3. Regions of existence of the two types of solitons (gray) in  $\epsilon$ - $\mu$  plane. The two separate regions are quite distinct. Parameters are shown in the plot. The hatched region corresponds to exploding solitons.

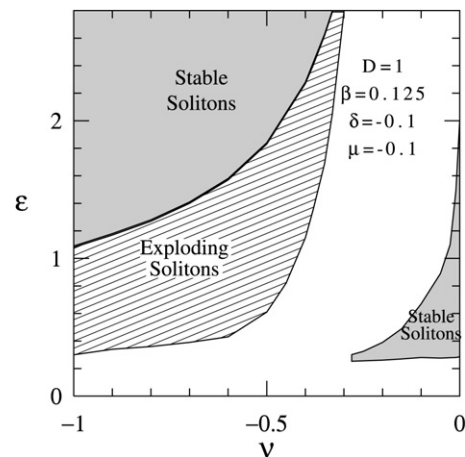


Fig. 4. Regions of existence of two types of solitons (gray) in  $(\epsilon, \nu)$  plane. Parameters are shown in the plot. The hatched region corresponds to exploding solitons.

results do not depend on the mesh intervals, thus avoiding any numerical artifacts.

Fig. 3, numerically obtained, shows regions in the  $(\mu, \epsilon)$  plane where stationary localized solutions can be found. As predicted by the simple model, there are two separate regions in the parameter space where dissipative solitons exist. The gray regions correspond to stable stationary solitons while the hatched region corresponds to exploding solitons [11–13]. A comparison between Fig. 1 and Fig. 3 shows that there is not only a qualitative agreement between them, but that they also coincide reasonably well quantitatively. Our simple model, of course, cannot describe the explosive instability that is related to many degrees of freedom of the CGLE solitons [13]. Thus, explosive solitons in a simple model will be in the area of stable fixed points. If we take this into account, the correspondence between the exact numerical results and the predictions of our simple model is remarkably close.

Fig. 4 compiles the results of numerical simulations of the CGLE for the plane of parameters  $(\nu, \epsilon)$ . Again, gray regions are for stable solitons while the hatched region is for explod-

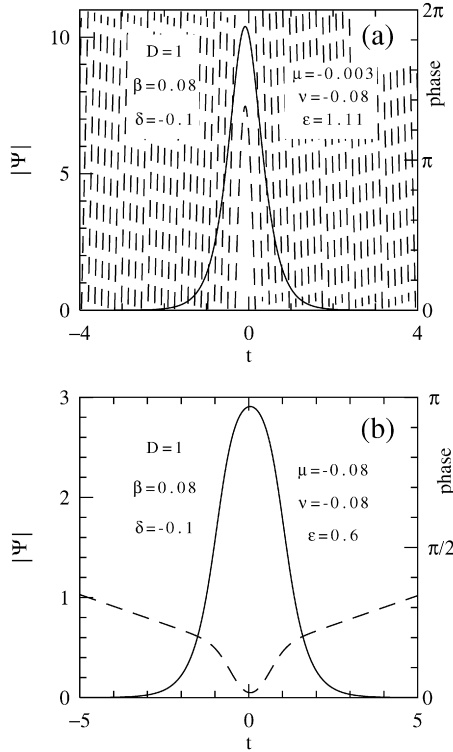


Fig. 5. Exact soliton profiles (solid lines) of two examples in the (a) upper and (b) lower regions in Fig. 4. They are marked by thick black dots in Fig. 4. Dashed lines show their corresponding phase profiles.

ing solitons. Comparing these results with those in Fig. 2 again shows a good qualitative agreement.

We have numerically calculated the exact field amplitude and phase profiles of the solutions for each region of existence of stable solitons. Two illustrative examples are presented in Fig. 5. The solid lines represent the field amplitude of the solitons, while the dashed lines are their phase profiles. The upper curves (a) in Fig. 5 correspond to the upper-right thick black point in Fig. 3 and vice versa: the lower curves (b) in Fig. 5 correspond to the lower-left thick black point. There are some obvious differences in the energies, widths and amplitudes of the two solitons. However, the most visible qualitative difference is in the soliton chirp. The phase profiles clearly show that the chirps in the two cases are of opposite sign. Due to this difference, the energy flows from the inside to the outside of the soliton in the first case while it flows inwards in the second case.

The results obtained from the reduced model (6) show that, for Fig. 1, the upper right corner region has  $\omega > 0$  and mostly  $c_0 > 0$  (and it is large in magnitude, i.e. there is a strong chirp across the soliton), while the stable FP on the lower left region has  $\omega < 0$  and  $c_0 < 0$  (and it is small in magnitude, so the soliton is weakly chirped). As regards Fig. 2, we have  $c_0 < 0$  (and  $\omega < 0$ ) in the lower right-hand corner region (low energy  $Q$ ), while we find  $c_0 > 0$  (and  $\omega > 0$ ) in the upper left corner region (high energy  $Q$ ). The same patterns for the chirp signs are obtained in the two distinct regions in Figs. 3 and 4 when directly solving the CGLE.

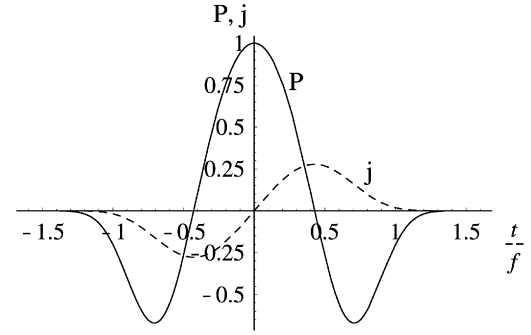


Fig. 6. Normalized density of energy generation  $P$  across the soliton (solid line) and normalized energy flux  $j$  (dashed line) for the reduced model with  $m = 1$ . If  $c_0 > 0$  then the curve shapes ( $\hat{P}$  and  $\hat{j}$ ) are as shown here (cf. Figs. 5(a) and 7(a)), so that energy is generated in the center. However, the curves are plainly inverted if  $c_0 < 0$ , and then the energy is dissipated in the center (cf. Figs. 5(b) and 7(b)).

We can use the reduced model to directly relate the chirp to the energy generation and flux. For stationary solutions, the density of energy generation,  $\hat{P}(t)$  is related to the flux,  $\hat{j}(t)$ , through the following equation (see Section 6 of [5]):

$$\hat{P}(t) = \frac{d\hat{j}}{dt}, \quad (7)$$

where

$$\hat{j} = \frac{i}{2}(\psi \psi_t^* - \psi_t \psi^*). \quad (8)$$

Using the trial function (5) for arbitrary  $m$ , we find the normalized flux

$$j(t) = \frac{\hat{j}}{2a^2(m)cQ} = T \exp\left[-2T^2\left(1 + \frac{T^2}{m}\right)\right], \quad (9)$$

where  $T = t/f$ . Then the normalized energy generation is given by

$$P(t) = \frac{\hat{P}f}{2a^2(m)cQ} = \left(1 - 4T^2 - \frac{8}{m}T^4\right) \exp\left[-2T^2\left(1 + \frac{T^2}{m}\right)\right]. \quad (10)$$

We have the condition that the total energy generation is zero:

$$\int_{-\infty}^{\infty} P(t) dt = 0. \quad (11)$$

This condition has to be satisfied for stationary solutions, and is clearly valid for these trial functions.

We plot  $P$  and  $j$  in Fig. 6. It is clear that  $\hat{P}$  and  $\hat{j}$  change sign with  $c$ , since they are proportional to  $c$ . Thus, the sign of the chirp has an important physical implication. If  $c_0 < 0$  then  $\hat{P} > 0$  in the wings and  $\hat{P} < 0$  around the pulse center. This means that energy is generated in the wings and flows towards the middle, where it is dissipated. Conversely, if  $c_0 > 0$  then  $\hat{P} < 0$  in the wings and  $\hat{P} > 0$  around the pulse center, so energy is generated in the middle and flows towards the wings, where it is lost. This process, involving an internal flux

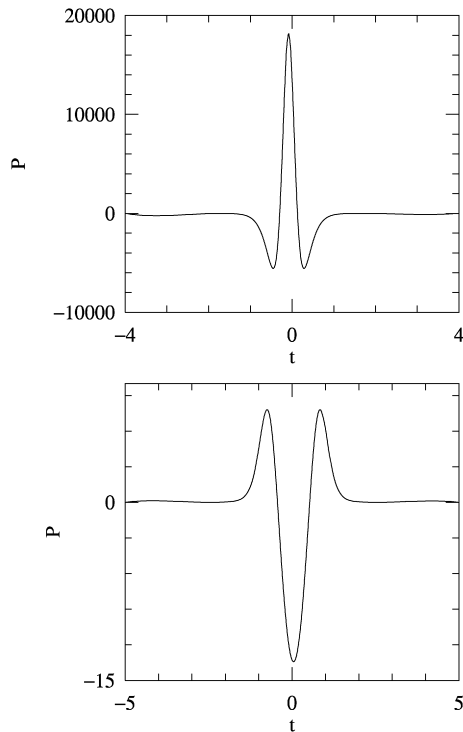


Fig. 7. Energy generation,  $P$ , inside the two types of solitons shown in Fig. 5. In (a) the energy is generated in the middle of the soliton and is dissipated in the tails while in (b) it is generated in the tails and dissipated in the center.

of energy, produces the dynamic equilibrium which we call a dissipative soliton.

The different signs of chirp and frequency offset ( $\omega$ ) appearing for each region (high  $Q$  and low  $Q$ ) mean that the phase profile across the soliton is concave up in one case, and concave down in the other. Hence we can designate them “solitons” and “antisolitons” for convenience. The phase profile for the CGLE solitons is not exactly parabolic, of course, but it is clear from Figs. 5(a) and 5(b) that the effective chirp coefficients are opposite in sign, and that the chirp magnitude in Fig. 5(a) is much greater than that in Fig. 5(b).

For comparison, we plot the distribution of energy  $P$  generated and dissipated inside of the CGLE soliton in Fig. 7. We can see clearly that in the first case (a), the energy generation is positive in the middle of the soliton and negative in the wings while in the second case (b), the energy is generated in the tails of

the soliton and dissipated in the middle. Thus, there is a fundamental qualitative difference between the two types of solitons. One type cannot be transformed into the other with a continuous change of parameters. To be specific, we call the solitons with lower energy and  $c_0 < 0$  (ordinary) dissipative solitons and the localized solutions of the upper branch (with  $c_0 > 0$ ) “dissipative antisolitons”.

In conclusion, we have shown that there are two types of stable fixed points in the reduced system representing dissipative solitons of the CGLE. The parameter regions of these solitons are disjoint. We have shown that these two types of solitons have opposite signs of the chirp parameter which governs the direction of energy flow inside the soliton. The predictions of the reduced approach have been confirmed by direct simulation of the CGLE.

### Acknowledgements

The authors acknowledge support from the Australian Research Council. The work of J.M.S.C. was also supported by the M.C.y.T. under contract FIS2006-03376.

### References

- [1] I. Aranson, L. Kramer, *Rev. Mod. Phys.* 74 (2002) 99.
- [2] D. Mihalache, D. Mazilu, F. Lederer, H. Leblond, B.A. Malomed, *Phys. Rev. A* 75 (2007) 033811.
- [3] H. Leblond, A. Komarov, M. Salhi, A. Haboucha, F. Sanchez, *J. Opt. A: Pure Appl. Opt.* 8 (2006) 319.
- [4] L. Pismen, *Patterns and Interfaces in Dissipative Dynamics*, Springer Series in Synergetics, Springer, 2006.
- [5] N. Akhmediev, A. Ankiewicz, *Dissipative solitons in the complex Ginzburg–Landau and Swift–Hohenberg equations*, in: N. Akhmediev, A. Ankiewicz (Eds.), *Dissipative Solitons*, Springer, Berlin, 2005.
- [6] See e.g. N. Akhmediev, A. Ankiewicz, *Solitons: Nonlinear Pulses and Beams*, Chapman & Hall, London, 1997.
- [7] A.I. Maimistov, *J. Exp. Theor. Phys.* 77 (1993) 727, *Zh. Eksp. Teor. Fiz.* 104 (1993) 3620 (in Russian).
- [8] M.N. Zhuravlev, N.V. Ostrovskaya, *J. Exp. Theor. Phys.* 99 (2004) 427, *Zh. Eksp. Teor. Fiz.* 126 (2004) 483 (in Russian).
- [9] E.N. Tsoy, N. Akhmediev, *Phys. Lett. A* 343 (2005) 417.
- [10] E.N. Tsoy, A. Ankiewicz, N. Akhmediev, *Phys. Rev. E* 73 (2006) 036621.
- [11] J.M. Soto-Crespo, N. Akhmediev, A. Ankiewicz, *Phys. Rev. Lett.* 85 (2000) 2937.
- [12] N. Akhmediev, J.M. Soto-Crespo, G. Town, *Phys. Rev. E* 63 (2001) 056602.
- [13] N. Akhmediev, J.M. Soto-Crespo, *Phys. Lett. A* 317 (2003) 287.